REGULAR PAPER

CrossMark

Real-time displacement measurement system using phase-shifted optical pulse interferometry: Application to a seismic observation system

Minoru Yoshida[1]*, Yoshiharu Hirayama[1]*, Atsushi Takahara[1], Motofumi Kashi[1], Keiji Takeuchi[1], Toshiharu Ikeda[1], Fumio Hirai[1], Yosuke Mizuno[2], Kentaro Nakamura[2], Hitoshi Kimura[3], Norio Ino[3], and Wataru Inoue[3]

[1]Hakusan Corporation, Fuchu, Tokyo 183-0044, Japan
[2]Precision and Intelligence Laboratory, Tokyo Institute of Technology, Yokohama 226-8503, Japan
[3]Department of Mechanical and Control Engineering, Tokyo Institute of Technology, Meguro, Tokyo 152-8552, Japan

*E-mail: yoshida@hakusan.co.jp; hirayama@hakusan.co.jp

We developed a method of detecting incident light levels on the oscillator surfaces and light pulses that include two interfering pulses with a phase shift of $\pi/2$ (phase-shifted optical pulse interferometry). This system enables the measurement of displacements greatly exceeding the half wavelength of the laser. Moreover, it allows measurements at multiple locations with a single optical fiber for using optical pulses. In this study, we conducted an interference experiment using 30 ns optical pulses and transmitted them at 1 µs intervals. We confirmed that the above two measurements are possible. Furthermore, from the data of the oscillator used for verification, we showed that measurements on the order of nanometers are possible. Since this method does not require a power supply to the oscillator, its widespread applications in physical exploration can be expected. © 2016 The Japan Society of Applied Physics

1. Introduction

In earthquake observation, ground motion is measured using an accelerometer and a velocity meter (called a seismometer); the measured data are used to determine the earthquake mechanism, ground structure, and internal structure of Earth.[1–3] Furthermore, when observing volcanoes, a seismometer is used to estimate the position and scale of a magma chamber to verify the mechanism of eruptions and predict volcanic eruptions.[4–6] To examine the mechanism of an earthquake hypocenter in detail, seismometers must be positioned around the epicenter. However, earthquakes associated with subducting plates often have epicenters in the ocean. Therefore, seismic observation only on land is insufficient, and earthquake observation networks have been installed on the sea floor around Japan as well as in other parts of the world.[7–9] In the field of geophysical exploration, which includes resource exploration, observations are made at multiple points in a wide area to improve the resolution. Therefore, in sea-floor exploration, sensors that do not require a power supply and a system that uses optical fiber for transmission are desired.[10,11]

There are several methods for measuring acceleration using optical fibers. For example, there are methods using the Fabry–Perot interferometer,[12,13] amplitude modulators,[14] and differential optical detectors;[15] others measure the vibration of a micromachine silicon cantilever with light-density modulation using multimode fibers,[16] involve fiber Bragg gratings (FBGs),[10,11,17–23] or are interferometric methods.[24–27] Among these, FBG[10,11,21] and interferometric[25] methods are primarily used for actualizing frequencies of 0.1 to several hundreds of Hz, which are necessary in earthquake observations including geophysical exploration, with a dynamic range of 100 dB.

FBG methods mainly use the measurement principle of a contact-type hydrophone, and optical fibers are wrapped around seismometers such as moving-coil-type seismometers. There exists a method to convert the vibration of the spindle inside a seismometer to the expansion and contraction of optical fibers to detect vibration;[10,11] another method uses the optical fiber itself as an accelerometer.[21] These methods do not require a power source between the fibers and the sensor; thus, they are currently used in sea-floor earthquake observation.

In the FBG methods,[28] it is generally necessary to use an FBG with a central reflection wavelength that is different in the number of multi points, although there are exceptions. Therefore, a wide-bandwidth light source that covers the entire wavelength range or a frequency-sweep light source is required, which is a disadvantage.

In contrast, interferometry enables measurement using a single-wavelength laser and is advantageous in that its sensitivity can be increased. For example, Zumberge et al.[25] measured the vibration of an STS1 seismometer in real time and conducted phase unwrapping. Assuming that an amplitude of several centimeters is captured with a resolution less than 1 pm, they showed that the performance of the STS1 seismometer can be maximized by light interferometry. The impact of these results was significant in the field of earthquake observation, especially as it presented a good prospect for high-precision observation that does not require a power source for the sensor. However, their proposed method uses continuous light; thus, creating multi points in the measurement system using a time-division multiplex is difficult.

In this paper, we propose phase-shifted optical pulse interferometry, which enables the easy integration of multiple observation points for application to a seismometer. Shindo et al.[29] provided a description of the method of using optical pulses and multiple observation points. In their interference method, they attached the fiber directly to the oscillator and observed the expansion and contraction of the oscillator during vibration using interference. Therefore, although a power supply is not required for the sensor, there is a disadvantage in that the oscillator amplitude cannot be measured beyond the half wavelength of the pulsed light.

Our method applies a pulse with a partial $\pi/2$ phase modulation to the front and back surfaces of a spring-suspended mass. When optical pulses are made to interfere by applying an appropriate delay on one side of the spring-

suspended mass, the light incident on the spring-suspended mass can also be measured and the changes in incident light intensity due to environmental fluctuations can be removed. Simultaneously, phase unwrapping becomes possible, which allows the measurement of a displacement that exceeds half the wavelength. A prototype of the spring-suspended mass was prepared, and a vibration measurement was conducted with the proposed light interferometry method to show that the measurement of a displacement that greatly exceeds the wavelength of the incident light is possible, as indicated by the principle. We also showed from the observation record of the spring-suspended mass that nanometer-order measurement is possible. Furthermore, by using a 30 ns optical pulse transmitted at 1 MHz, we conducted a simultaneous experiment for the two sensors to show that measurement at multiple locations is possible. For this transmission condition, measurement with up to 20 sensors is possible in a calculation.

2. Phase-shifted optical pulse interferometry

Generally, to measure the interference signal obtained through light interferometry, the phase difference θ between the reference light r and the measurement light s is obtained. The electrical signal level I of interference light i resulting from interference between the reference light r and measurement light s is expressed as

$$I = |r + s|^2 = R + S + 2\sqrt{RS}\cos\theta. \tag{1}$$

At this time, R, S, and I are the electric signal level of the reference light r, measurement light s, and interference light i, respectively, which are equal to the square of the effective amplitude of each light. In the conventional method, R and S are treated as constants; therefore, the variation error due to intensity fluctuation on the transmission pathway could not be separated, implying that the conventional method is unsuitable for a measurement that requires long-term stability, such as a field observation. In the present study, the light signal was pulsed and made to interfere with the reference light by appropriately delaying the measurement light. This allows for a design in which the interference output pulse can be obtained as a time-division multiple pulse of the portion of the reference light only R, interference light portion I where the reference light and measurement light overlap, and the portion of the measurement light only S. Thus, the electric signal levels R, I, and S can be obtained simultaneously. Consequently, $\cos\theta$ can be obtained using Eq. (1).

Questions that use Eq. (1) are output with $\cos\theta$ ranging from -1 to 1; however, because the measurement error is so large that $|\cos\theta|$ is closer to 1, it is necessary, in practice, to take measurements within the range of $|\cos\theta| < 1/\sqrt{2}$, where good linearity exists. Therefore, a light accelerometer with an automatic drift compensation function built into the light source has already been created so that θ is constantly around $\pi/2$.[30] However, in this method, only a displacement shorter than half the wavelength can be measured, limiting the dynamic range.

The method proposed in the present study allows for continuous measurement without adjusting the phase of the light source. Two pulses with phases differing by $\pi/2$ are used, as shown in Fig. 1(a). The reference light interferes with the measurement light, which is delayed by τ, to obtain two interference outputs, namely, I_1 and I_2, in addition to R and S.

(a)

(b)
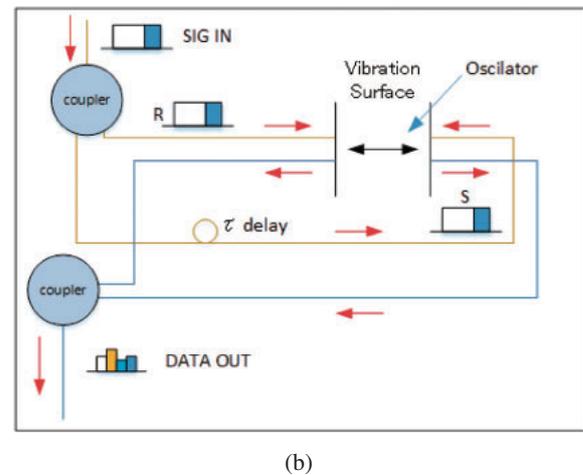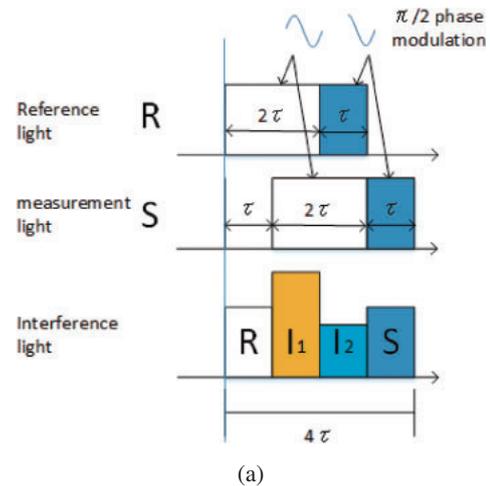
Fig. 1. (Color) (a) Schematic diagrams of reference light, measurement light, and interference light. (b) Schematic diagram of phase-shifted optical pulse interferometry.

If the input pulse length in Fig. 1(a) is 3τ, $\pi/2$ phase modulation is applied only to the final τ. Through interference resulting from applying a delay τ to the input pulse on one side of the vibration plane, an output pulse with length 4τ is obtained. At this time, the following holds:

$$\cos\theta_1 = \frac{(I_1 - R - S)}{2\sqrt{RS}}, \tag{2}$$

$$\cos\theta_2 = \frac{(I_2 - R - S)}{2\sqrt{RS}}, \quad \theta_2 = \theta_1 - \frac{\pi}{2}. \tag{3}$$

By taking the ratio of (2) and (3),

$$\frac{\cos\theta_2}{\cos\theta_1} = \frac{\sin\theta_1}{\cos\theta_1} = \tan\theta_1 = \frac{(I_2 - R - S)}{(I_1 - R - S)}. \tag{4}$$

Therefore,

$$\theta_1 = \tan^{-1}\left(\frac{I_2 - R - S}{I_1 - R - S}\right) = \cot^{-1}\left(\frac{I_1 - R - S}{I_2 - R - S}\right). \tag{5}$$

Hereafter, θ_1 will be written as θ.

In the tangent function, θ diverges at $\pm\pi/2$, while in the cotangent function, θ diverges at 0 and π. To avoid these divergence points, we chose the function with the absolute value closer to 0 in order to calculate θ in the range $-\pi \le \theta < \pi$ as follows:

$$\theta = \begin{cases} \tan^{-1}\left(\dfrac{I_2 - R - S}{I_1 - R - S}\right) & \text{when } \left|\dfrac{I_2 - R - S}{I_1 - R - S}\right| \leq 1 \\[3mm] \cot^{-1}\left(\dfrac{I_1 - R - S}{I_2 - R - S}\right) & \text{when } \left|\dfrac{I_2 - R - S}{I_1 - R - S}\right| > 1 \end{cases}. \quad (6)$$

The variation $\Delta\theta(t)$ at a time t is calculated from θ obtained for every sampling interval Δt:

$$\Delta\theta(t) = \theta(t) - \theta(t - \Delta t). \quad (7)$$

When the above value exceeds π, 2π is subtracted; when the value is below $-\pi$, 2π is added for adjustment.

The variation $\Delta\theta(t)$ is the quadruple of the phase difference caused by the amplitude of the actual oscillator. As shown in Figs. 1 and 5, this is due to the interference of light that was measured on both sides of the oscillator.

If θ' is assumed as $\Delta\theta$ when the sampling interval Δt is sufficiently small, the actual phase change $\Theta(t)$ is calculated as

$$\Theta(t) = \int_0^t \theta' \, dt. \quad (8)$$

The calculated displacement $D(t)$ can be obtained by multiplying $\Theta(t)$ by the wavelength of the measurement light λ as

$$D(t) = \frac{\lambda}{2\pi} \int_0^t \theta' \, dt. \quad (9)$$

In this method, as long as the measurement is within range, there is no limit to the number of phase unwrapping steps. We call this interferometry as phase-shifted optical pulse interferometry.

3. Spring-suspended mass as an accelerometer

3.1 Measurable range

The condition that enables phase unwrapping through phase-shifted pulse interferometry allows for the determination of the vibration direction with $\Delta\theta$; thus,

$$|\Delta\theta(t)| < \frac{\pi}{2}, \text{ i.e., } |\Delta D(t)| < \frac{\pi}{2} \times \frac{\lambda}{2\pi} = \frac{\lambda}{4} \quad (10)$$

must be true.

At this point, let us assume that the spring-suspended mass vibrates at the displacement $d(t) = A\sin(2\pi ft)$. The maximum displacement rate of this spring-suspended mass $d(t)_{max}$ is $2\pi fA$. Therefore, the maximum change in displacement, $|\Delta d(t)|$, with the sampling rate of the laser light F (Hz) is $2\pi Af/F$. As we will discuss in Sect. 4.1, if the design allows for interference with a reflected wave on applying an optical pulse from both sides of the spring-suspended mass, the light path of the optical pulse $D(t)$ becomes four times the actual displacement of the spring-suspended mass $d(t)$. Therefore, the condition for the maximum amplitude of the measurable spring-suspended mass A and frequency f is

$$|\Delta D(t)| = |4\Delta d(t)| = \frac{8\pi Af}{F} < \frac{\lambda}{4}. \quad (11)$$

Since this system is a magnifying structure, it is possible to enlarge fine fluctuations and capture them. Hence, it has the advantage of precision.

If the wavelength and sampling rate of the laser light used are 1.55 μm and 1 MHz, respectively, the amplitude A must
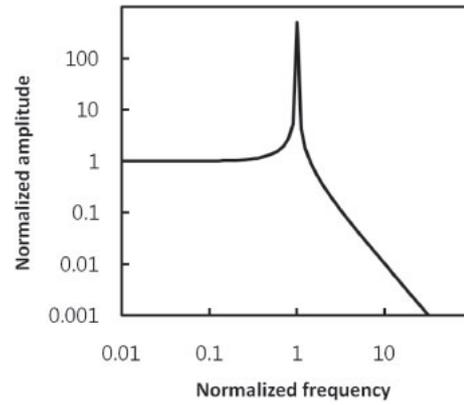
Fig. 2. Amplitude characteristics of an accelerometer.

be less than $1.55/(32\pi f)$ m. For example, it is possible to observe a vibration with $f = 10$ Hz as long as the amplitude A of the spring-suspended mass is less than 1.5 mm.

3.2 Preparation of the spring-suspended mass as an accelerometer

To apply the phase-shifted optical pulse interferometry to the observation of vibrations such as earthquakes, we prepared a spring-suspended mass as an accelerometer. When measuring vibrations such as ground motions using a spring-suspended mass, a damping force proportional to the velocity of the spring-suspended mass is typically applied. The equation of motion for such a system is[31]

$$\frac{d^2y}{dt^2} + 2\gamma\frac{dy}{dt} + \omega_0^2 y = \frac{d^2x}{dt^2}, \quad (12)$$

where y is the relative displacement of the spring-suspended mass, $\gamma\ (= h\omega_0)$ is the attenuation rate, h is the attenuation constant, ω_0 is the natural angular frequency of the spring-suspended mass, and x is the displacement input from outside.

The frequency characteristics of a seismometer are generally expressed as a response when a sine-wave ground motion is applied. Considering $x(t) = \sin\omega t$ with $\omega = 2\pi/T$, we obtain

$$y(t) = U(\omega)\sin[\omega t + \delta(\omega)], \quad (13)$$

where

$$U(\omega) = \frac{\omega^2}{\sqrt{(\omega_0^2 - \omega^2)^2 + 4\gamma^2\omega^2}} \text{ and } \tan\delta = \frac{-2\gamma\omega}{\omega_0^2 - \omega^2}.$$

Regarding the amplitude in Eq. (13), the normalized displacement amplitude of the spring-suspended mass is expressed in a graph with a normalized frequency (Fig. 2). If $\omega \ll \omega_0$, the amplitude of $y(t)$ does not depend on the input frequency, but instead takes a value depending on the input acceleration.

In actual seismometers, the damping factor is of the order of 0.7 to prevent an increase in vibration near the natural frequency of the oscillator. In the case of detecting ground displacement, the region of $\omega \gg \omega_0$ is used, and in the case of detecting ground acceleration, the region of $\omega \ll \omega_0$ is used. Considering ours as a device for system verification, we used the region of the accelerometer where the oscillator is not damped and conducted the verification.
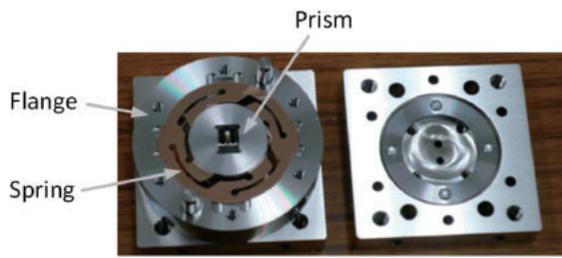
Fig. 3. (Color) Inside of the spring-suspended mass (with the outer flange removed).
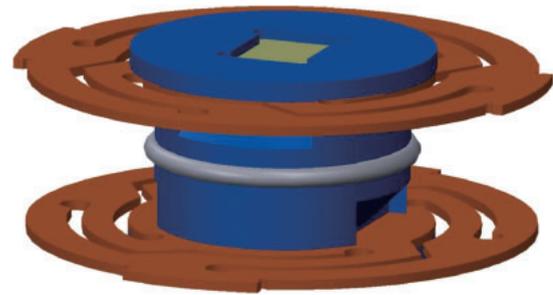
Fig. 4. (Color) 3D CAD model of the vibrating part in the sensor.
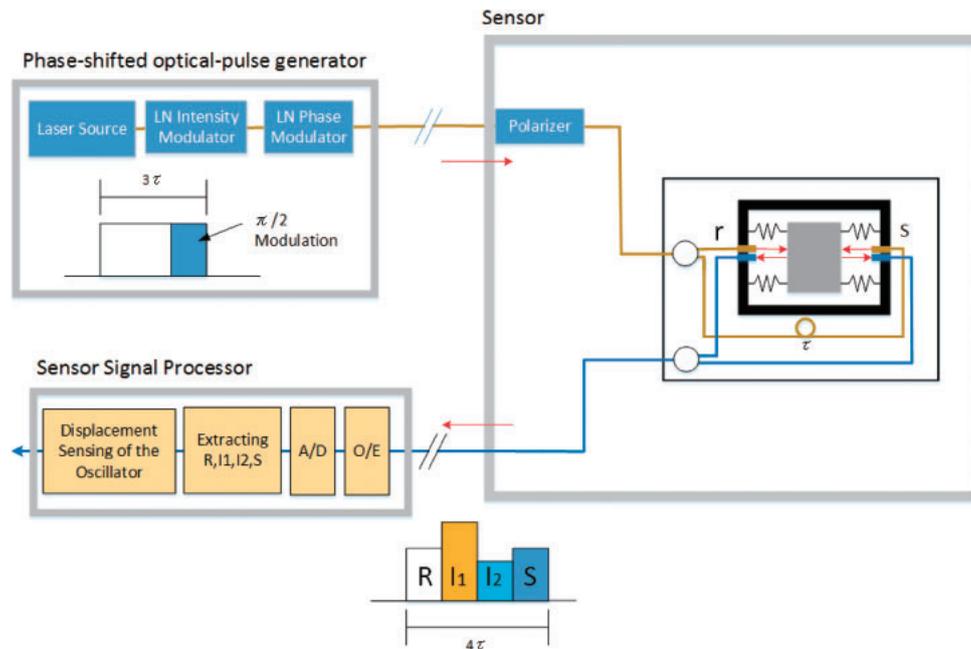
Fig. 5. (Color) Structure of the test bed in phase-shifted optical pulse interferometry. This method uses laser-pulse inputs R and S. The pulse duration is 30 ns. The phase of the last 10 ns is progressed (regressed) to $\pi/2$ against the first 20 ns. This pulse is transmitted every 1 μs.

In a typical earthquake observation, measurements are taken at 100 Hz or lower; therefore, a spring-suspended mass is prepared with a natural frequency of approximately 300 Hz, along with that with a natural frequency of approximately 50 Hz to verify the measurements of large amplitudes at the low frequency by phase-shifted optical pulse interferometry.

Sensor parts of the spring-suspended mass with a natural frequency of approximately 300 Hz are shown in Fig. 3. The outer shape of the sensor prepared for this study consists of nickel-plated brass, and the total size of the sensor is 36×36 mm². The spring of the sensor is made of beryllium copper, and is the outer diameter is 25ϕ.

A three-dimensional (3D) computer aided design (CAD) model of the vibrating part in this sensor is shown in Fig. 4. The spring characteristics in the design of this model were as follows: through mode analysis with the peripheral portion of the spring fixed, the primary mode was vertical against the plane of the spring, and the natural frequency was 371 Hz.

4. Spring-suspended mass measurement system

4.1 System structure

By using the principle of phase-shifted optical pulse interferometry presented in Sect. 2, we prepared a test bed

that measures the vibration of the spring-suspended mass discussed in Sect. 3. This system consists of a phase-shifted optical pulse generator, a sensor signal processor, and a sensor connected to the tip of an optical fiber (Fig. 5).

In the phase-shifted optical pulse generator, a continuous light of 1.55 μm wavelength was generated as the interference light source by using a highly stable laser transmitter with a narrow line width of 5 kHz. A high-speed lithium niobate (LN) intensity modulator and an LN phase modulator that can provide GHz-band behavior were used for the laser light, and an optical pulse with a total pulse width of 30 ns and a relative phase difference of $\pi/2$ at 20 ns to the front and 10 ns to the back was generated and transmitted at 1 μs intervals.

A polarization-maintaining fiber was used for transmission to the sensor. At the sensor, the optical pulse is branched by couplers after passing through a polarizer. After reflecting on reflexive mirrors attached to both sides of the spring-suspended mass, the light interferes and enters the sensor signal processor.

The sensor signal processor converts the light signal into an electric signal, and subsequently conducts A/D conversion at a sampling rate of 3.6 GHz, extracting the interference pulse at intervals of 1 μs to obtain R, S, I_1, and I_2. Next, it calculates the displacement from $\Delta\theta$ of the spring-

suspended mass that has gone through 2000th-order moving-average processing, and it outputs with 1 MHz sampling.

A frequency band of 200 Hz or less is used in the field of natural earthquakes and physical exploration. Therefore, as the preliminary processing of the obtained data, we applied a comb filter that cuts off frequencies above 500 Hz. Since this study involves 1 MHz sampling data, we decided to take a 2000th-order moving average.

4.2 Vibration experiment

An anti vibration table was installed for the vibration experiment. A metal box containing gel was placed on this table, and the vibration table was placed on top of this box. As we aimed to obtain the value of acceleration actually applied to the spring-suspended mass, the servo-type accelerometer JA40GA manufactured by Japan Aviation Electronics Industry, Ltd. was also set on this table to adjust the input of the vibration table. JA40GA is an accelerometer often used for earthquake observations in Japan[32] and is flat from 0 to approximately 200 Hz, allowing measurements up to $\pm 39.6 \, \text{m/s}^2$.[33]

The spring-suspended mass from Sect. 3 was placed on the vibration table. Figure 6(a) shows a Lissajous figure obtained with the 1 MHz sampling of a sine wave at an acceleration rate of 2.94 m/s^2, a frequency of 30 Hz, and an observation time of 0.05 s. $\cos\theta_1$ and $\cos\theta_2$ were calculated using Eqs. (2) and (3), respectively. The Lissajous figure shows a change along a true circle.

In our system, we conducted the experiment by adjusting the phase shift of the pulse to be $\pi/2$ in the phase-shift cycle of the pulse, causing a circular display of the Lissajous figure, as shown in Fig. 6(a), and by simultaneously confirming it. When we used the ellipse fitting method[34] for the Lissajous figure in Fig. 6(a), the major axis of the ellipse was 0.999, the minor axis was 0.965, and the major axis/minor axis ratio was 1.03. In addition, the tilt of the ellipse was 0.1 rad, and we could confirm that the Lissajous figure is almost a circle.

Therefore, it is confirmed that the $\pi/2$ phase shift of the incident pulse was achieved; i.e., the phase difference between θ_1 of Eq. (2) and θ_2 of Eq. (3) is $\pi/2$. Furthermore, we can see that the transfer at 2π, which exceeds the wavelength of the laser light in Eq. (8), is appropriately achieved. $\Delta\theta$ in Fig. 6(b) was obtained by applying a 2000th-order moving average to the results of Eq. (7), and the amplitude roughly changed with a sine wave of 0.003 rad, confirming that the measurements were within the limit stipulated by Eq. (10).

In Fig. 6(c), the displacement of the spring-suspended mass is approximately 1 μm, and the frequency is 30 Hz. As shown in Figs. 6(a) and 6(b), the measurements are appropriate; thus, the displacement in Fig. 6(c) expresses the actual displacement of the spring-suspended mass. This is a result of the oscillator used in this study, and when the parameters of the oscillator used such as resonant frequency and Q-value change, the maximum acceleration also varies.

4.3 Consistency of light interferometer record by inputting a square wave

Next, a square wave of 0.1 Hz frequency was input into the vibration table, and a single-degree-of-freedom attenuating vibration was measured. The displacement of the vibration table that uses a laser displacement meter and the acceleration
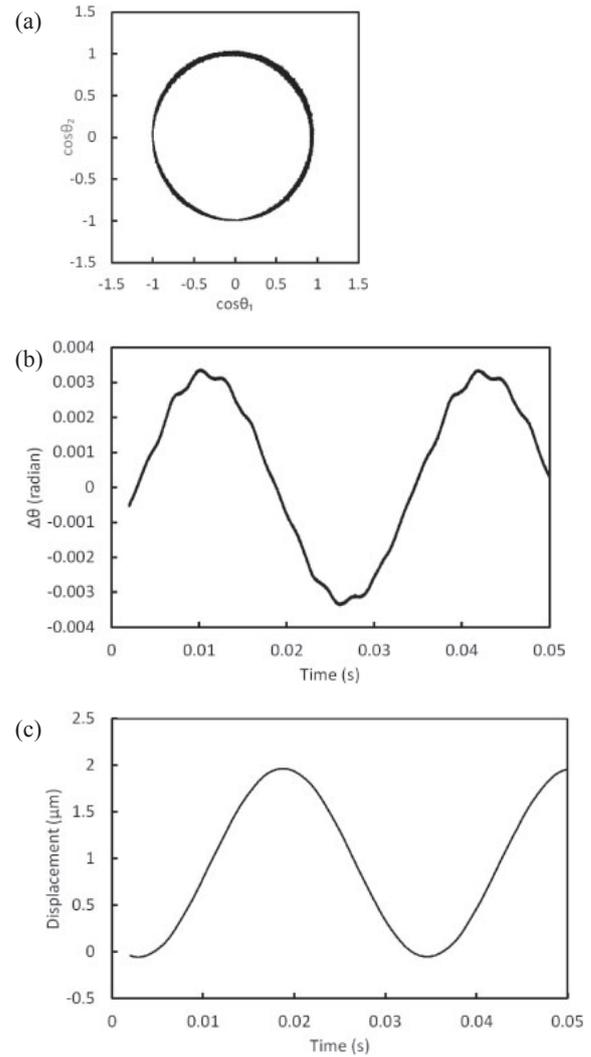
Fig. 6. (a) Lissajous figure for $\cos\theta_1$ and $\cos\theta_2$. (b) Values of $\Delta\theta$. (c) Waveforms obtained by integrating (b).

of the vibration table with a servo accelerometer were simultaneously measured using one data logger with 1 kHz sampling. We examined the consistency with the displacement of the spring-suspended mass with light interferometry obtained at 1 MHz sampling and detected small, free natural vibrations.

Figure 7(a) shows the acceleration of the vibration table measured using the servo accelerometer and the displacement of the sensor measured using light interferometry when a square wave of 0.1 Hz frequency and 0.55 mm amplitude was input. Figure 7(b) shows the overlapping Fourier spectrum for each measurement.

The damping ratio ζ calculated from the envelope of the sensor displacement shown in Fig. 7(a) was 0.05027. As the attenuation is small, the displacement of the spring-suspended mass will show a natural vibration of the sensor on the line proportional to the input acceleration. The graph showing an overlap with the acceleration measured using the accelerometer at the same time indicates that the measured displacement of the spring-suspended mass agrees with the theory, implying that our technique provides correct measurements [Fig. 7(a)]. The graph showing the Fourier spectrum for each measurement [Fig. 7(b)] further confirms the validity of the interferometry technique. When Fourier
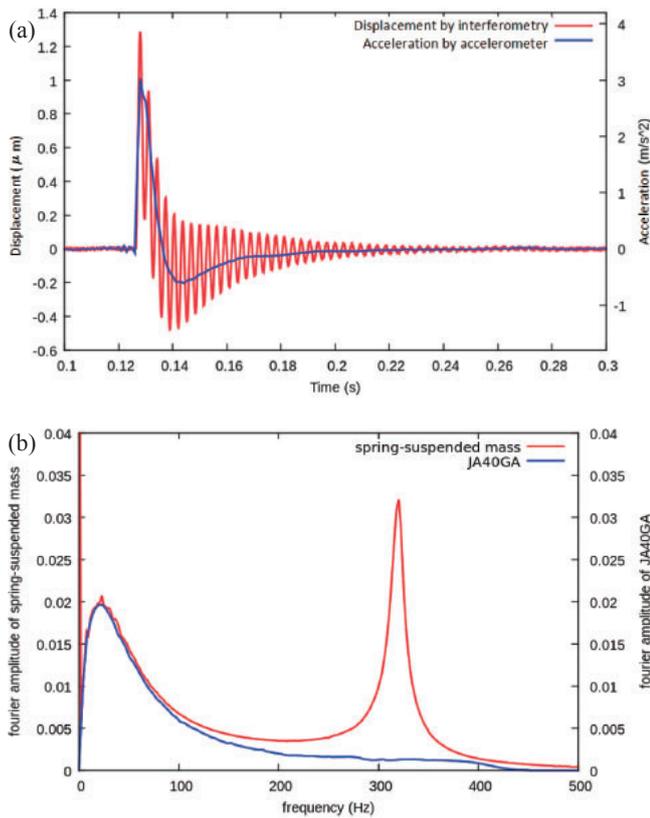
Fig. 7. (Color) (a) Acceleration measured using the accelerometer and displacement of the sensor obtained using light interferometry. (b) Fourier spectra of the accelerometer and spring-suspended mass.

analysis was conducted on the displacement of the spring-suspended mass, the natural frequency was 320 Hz. This is approximately 15% off the design value of 371 Hz indicated in Sect. 3.2. The reason for this difference is that the spring-suspended mass is not completely fixed, and the spring constant is lower than the calculated value.

Next, to confirm that the spring-suspended mass captures displacements with small free vibrations, we show the measurement values from approximately 0.3 s after adding a square-wave displacement (Fig. 8). Figure 8(a) shows the Lissajous expressions of $\cos \theta_1$ and $\cos \theta_2$ calculated using Eqs. (2) and (3), which indicate that the phase barely changed. Figure 8(b) shows $\Delta\theta$ obtained by applying a 2000th-order moving average taken for a duration of 0.01 s from approximately 0.3 s after adding a square-wave displacement. The obtained $\Delta\theta$ shows sine-wave oscillation with an amplitude of 20 μrad. The optical path difference of the laser light was four times $\Delta\theta$, indicating that the 5 μrad variation in the displacement difference of the spring-suspended mass is captured. If the path difference is expressed as a length, that is as the wavelength of the laser light of 1.55 μm, it is $1.55 \times [5 \times (10^{-6}/2\pi)] = 1.2 \times 10^{-6}$ μm; thus, this system has the ability to capture a displacement of 1.2 pm. The displacement in Fig. 8(c) obtained using Eq. (9) is affected by the integral at both ends, but the measurement captures the displacement of a natural vibration with an amplitude of approximately 1.5 nm. In addition, when we took the time variation obtained from the laser displacement meter as the input quantity, carried out a dynamic simulation of the mass-spring damper system, and determined the
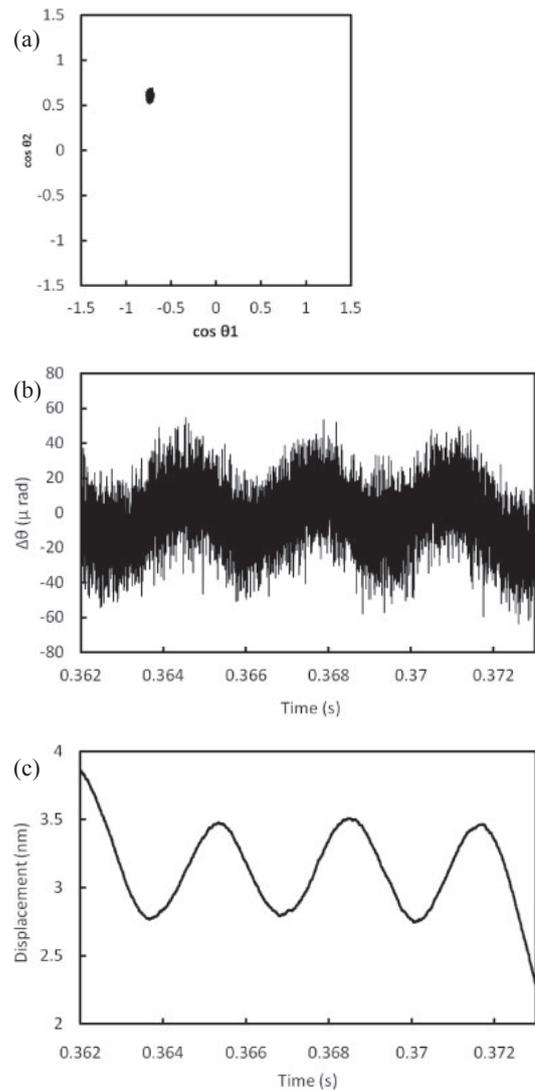
Fig. 8. (a) Lissajous figure for a duration of 0.01 s approximately 0.3 s after inputting a square wave displacement. (b) 2000th-order moving average for $\Delta\theta$ for a duration of 0.01 s approximately 0.3 s after inputting a square-wave displacement. (c) Waveform of the displacement obtained by integrating $\Delta\theta$.

displacement with respect to the housing of the optical sensor, we confirmed that it matched well with the output value of the optical sensor.

4.4 Connecting multiple spring-suspended masses
In addition to the structure presented in Sect. 4.1, the optical pulse was branched using a coupler. By delaying one branch, we can show that two spring-suspended masses can be measured with time division.

In the optical pulse generator, the optical pulse with a width of 30 ns was prepared as indicated in Sect. 4.1 and transmitted with 1 μs intervals. In the sensor, light passes through a polarizer and is branched using a coupler. One branch of the pulse is reflected at reflexive mirrors attached to both sides of the spring-suspended mass, as in the previous section, and then made to interfere. The other branch of the pulse is delayed by 50 ns, and then the wave reflected from the spring-suspended mass interferes in the same manner. With this delay, the interference pulse from two spring-suspended masses is transmitted to the signal processor with
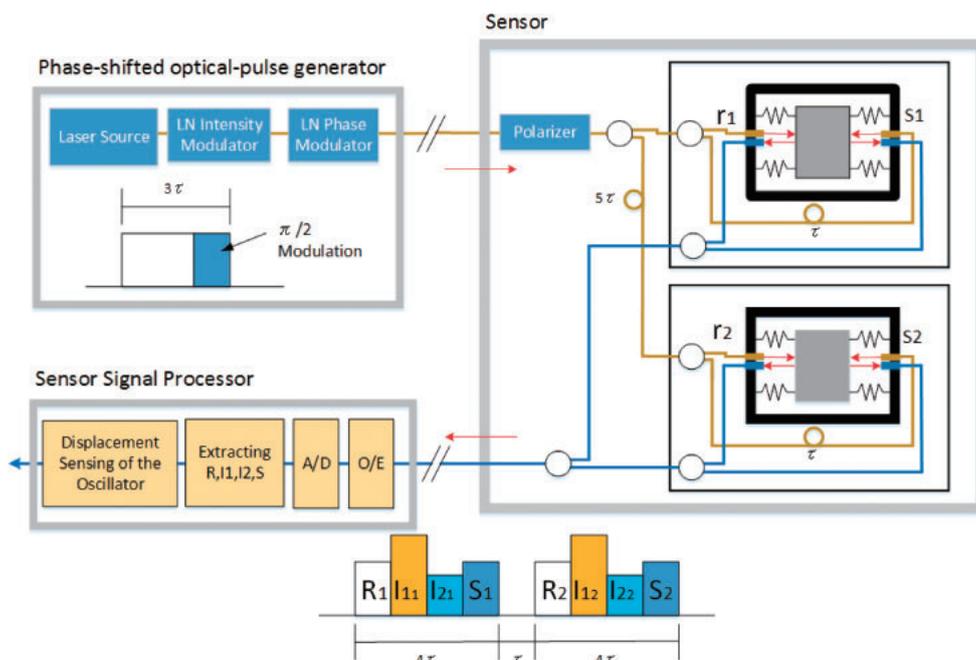
Fig. 9. (Color) Configuration diagram of the test bed when conducting simultaneous multiple observations with phase-shifted optical pulse interferometry. This method uses laser-pulse inputs R and S. The pulse duration is 30 ns. The phase of the last 10 ns is progressed (regressed) to $\pi/2$ against the first 20 ns. This pulse is transmitted every 1 µs.
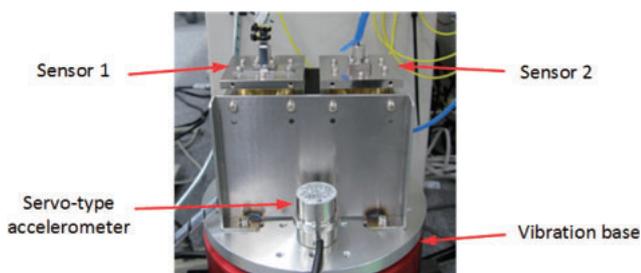
Fig. 10. (Color) Photograph of the spring-suspended mass and sensor during observations.

Fig. 11. (Color) (a) Output waveform obtained during simultaneous vibration. (b) Fourier spectra obtained during simultaneous vibration.

a 10 ns shift; thus, the components can be sequentially output without interference with each other (Fig. 9).

In this experiment, two spring-suspended masses with a natural frequency of approximately 50 Hz are installed on the vibration table and forced to vibrate at 35 Hz. If the parameters other than the natural frequency of the spring-suspended masses are the same, a spring-suspended mass with a lower natural frequency will show a higher amplitude. The amplitude of the 50 Hz spring-suspended mass is higher than that of the 320 Hz spring-suspended mass; therefore, while simultaneous observations were made for the two spring-suspended masses, their amplitudes were also verified. A photograph of the observation is shown in Fig. 10. The red part at the bottom of Fig. 10 is the vibration base that moves up and down. The sensor in the front is the servo-type accelerometer, and the two parts lined on the top are the spring-suspended masses. These spring-suspended masses can simultaneously vibrate on one vibration table.

The observation results were processed in the same manner as before, and the displacement waveforms [Fig. 11(a)] and spectra [Fig. 11(b)] of the spring-suspended masses were identified. Figure 11(a) indicates that the frequencies of the

two spring-suspended masses are in agreement, but the displacement amplitudes are different.

Since the parts containing the spring are not exactly the same, there is a possibility that an error may have occurred in the thickness and length; since the oscillator configuration is not completely fixed, it is likely that variations have occurred. Since the objective of the current study is to check the
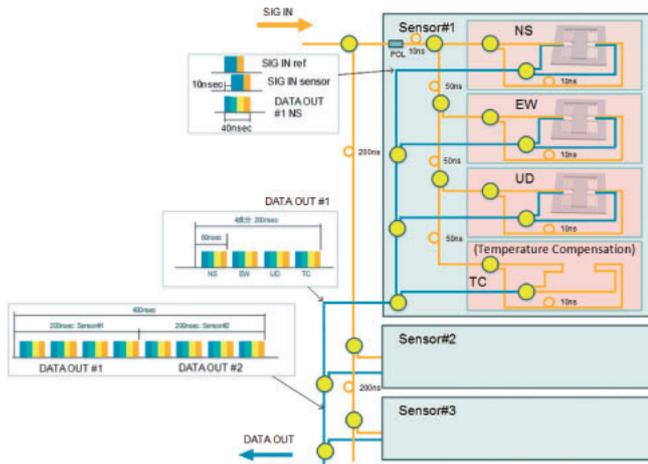
Fig. 12. (Color) Schematic diagram of multiple observation points.

behavior under multiple sensors, the uniformity of sensor performance has not been focused upon. However, since the homogeneity of the oscillator performance is important for future practical applications, we would like to resolve this issue in the future.

The Fourier spectra in Fig. 11(b) indicate that, for an input of 35 Hz, two spring-suspended masses respond in the same manner, showing that the simultaneous measurement of two spring-suspended masses through the interferometry technique was successful. When simultaneously measuring two sensors, an approximate loss of 3 dB is caused by optical pulse branching, but it does not affect the accuracy of the measurements. If multiple points are used, the effect of the loss can be removed by increasing the amplification of the light in the system.

The seismometer typically requires three components at one observation station: north–south, east–west, and up–down. Furthermore, in this system, a compensation circuit is inserted to remove the disturbances other than the spring-suspended mass, implying that there is one observation point with four components.

If a pulse with $\tau = 10$ ns is transmitted from the pulse generator at 1 µs intervals, as in Fig. 12, a period of 200 ns is necessary in the four components. By applying 200 ns for each observation point, multiple observation points can be connected using the same optical fiber. Under these conditions, at the maximum in a calculation, the interference pulse of five observation points and 20 sensors can fit within 1 µs, enabling the installation of five observation points using one fiber.

5. Discussion

As shown in Fig. 12, we constructed this system to reduce the system noise and environmental noise by simultaneously measuring the records of fixed ends and subtracting these records from the record of each sensor. Incidentally, the observation records with the fixed ends showed that the noise is low in high-frequency regions with frequencies higher than 1 Hz and in low-frequency regions with frequencies lower than 1 Hz; the noise increased with the decrease in frequency. Next, when the two fixed ends were simultaneously measured, their noise levels were almost the same over the entire frequency, and the noise levels obtained from the difference

between the two showed an improvement of approximately 20 dB over the entire frequency range when compared with the noise levels separately obtained from the individual fixed ends. However, the spectral shape remains nearly unchanged from the spectral shapes of individual fixed ends, and we found that the increasing trend of noise in the low-frequency regions cannot be eliminated. Since the noise reduction in the low-frequency regions is directly connected to the practical applicability of the broadband seismometer, an improvement in this area is a major challenge for the future.

On the other hand, if the vibration of the geophone can be directly measured using the proposed interferometry technique, a more detailed vibration measurement at the sensor without a power supply can be realized in comparison with that achieved in the previous study, in which the displacement in the spring-suspended mass vibration in the geophone was measured as a change in capacitance by using the electric signal.[35,36]

By using the phase-shifted optical pulse interferometry proposed in this paper, the signal levels of reference light, R, measurement light, S, and interference light, I, can be simultaneously measured to remove the loss in the light-signal path, enabling application in long-distance transmission. Furthermore, by delaying the light-receiving interval of the pulse for each sensor, multiple channel measurements by the same pulse become possible. Therefore, one can consider the output for temperature compensation and connect multiple sensors with ease. This characteristic will lead to a long-term and real-time monitoring network of resources without a power supply and a seismogram for deep drilling at high temperatures. In this study, we performed measurements using the 30 ns pulse transmitted at 1 MHz. Under these conditions, up to 20 components can be measured using one light source. In the future, by decreasing the optical pulse length to one-fifth, the maximum number of measureable components can be increased to 100. Data output in this study was performed at a high speed (1 MHz sampling), and in the decimation process, measurements at 1 kHz sampling indicated potential for resource exploration and those at 100 Hz sampling indicated potential for earthquake observation.

6. Conclusions

We examined the principle of phase-shifted optical pulse interferometry and showed that measurements using our prototype spring-suspended mass of distances significantly exceeding the wavelength of the incident light are possible, as suggested by the principle. On the basis of the record of spring-suspended mass observation, we showed that measurements on the order of nanometers are possible. Furthermore, by using an optical pulse with a length of 30 ns transmitted at 1 MHz, we conducted a simultaneous vibration experiment of two sensors and showed that measurement at multiple locations with one optical path is possible. In the future, by using a suitable spring-suspended mass, we plan to develop an optical seismometer that is practical for field use.

Acknowledgements

1) K. Aki and P. G. Richards, *Quantitative Seismology* (University Science Books, Sausalito, CA, 2002) 2nd ed., Chap. 12.
2) T. Lay and T. C. Wallace, *Modern Global Seismology* (Academic Press, London, 1995) p. 519.
3) W. H. K. Lee, H. Kanamori, P. C. Jennings, and C. Kisslinger, *International Handbook of Earthquake and Engineering Seismology* (Academic Press, London, 2002) p. 1915.
4) M. Iguchi, Kazan **58**, 1 (2013) [in Japanese].
5) K. Aki, M. Fehler, and D. Shamita, J. Volcanol. Geotherm. Res. **2**, 259 (1977).
6) B. A. Chouet, Nature **380**, 309 (1996).
7) Seafloor Observation Network for Earthquakes and Tsunamis along the Japan Trench (S-net) (National Research Institute for Earth Science and Disaster Prevention) [http://www.bosai.go.jp/inline/] [in Japanese].
8) Dense Oceanfloor Network System for Earthquakes and Tsunamis (DONET) — Concentrates Observation System for an Anticipated Tonankai Earthquake (Japan Agency Marine-Earth Science and Technology) [https://www.jamstec.go.jp/donet/e/].
9) Neptune Canada: seismograph network [http://www.neptunecanada.ca/news/multimedia-gallery/presentations/workshop-2-09/seismology-network-update.dot].
10) H. Nakstad and J. T. Kringlebotn, Proc. SPIE **7004**, 700436 (2008).
11) J. T. Kringlebotn, H. Nakstad, and M. Eriksrud, Proc. SPIE **7503**, 75037U (2009).
12) A. D. Kersey, D. A. Jackson, and M. Corke, Opt. Commun. **45**, 71 (1983).
13) A. S. Gerges, T. P. Newson, J. D. C. Jones, and D. A. Jackson, Opt. Lett. **14**, 251 (1989).
14) J. Kalenik and R. Pajak, Sens. Actuators A **68**, 350 (1998).
15) V. Mohanan, B. K. Roy, and V. T. Chitnis, Appl. Acoust. **28**, 95 (1989).
16) J. Marty, A. Malki, C. Renouf, P. LeCoy, and F. Baillieu, Sens. Actuators A **47**, 470 (1995).
17) P. Ferraro and G. De Natale, Opt. Lasers Eng. **37**, 115 (2002).
18) G. Gagliardi, M. Salza, P. Ferraro, P. De Natale, A. Di Maio, S. Carlino, D. De Natale, and E. Boschi, Meas. Sci. Technol. **19**, 085306 (2008).
19) P. F. da Costa Antunes, H. F. T. Lima, N. J. Alberto, and H. Rodoigues, IEEE Sens. J. **9**, 1347 (2009).
20) A. Laudati, F. Mennella, M. Esposito, A. Cusano, M. Giordano, G. Breglio, S. Sorge, C. C. Tassini, A. Torre, G. D'Altrui, and A. Cutolo, Proc. SPIE **6619**, 66191C (2007).
21) H. Y. Au, S. K. Khijwania, and H. Y. Tam, Proc. SPIE **7004**, 70042S (2008).
22) Y. Zhang, J. Ning, T. Koscica, H. Li, and H. L. Cui, ITEA J. **30**, 455 (2009).
23) B. N. P. Paulsson, J. L. Toko, J. A. Thornburg, F. Slopko, R. He, and C. Zhang, Proc. 38th Workshop Geothermal Reservoir Engineering, 2013, p. 11.
24) M. A. Zumberge, J. Berger, M. A. Dzieciuch, and R. L. Parker, Appl. Opt. **43**, 771 (2004).
25) M. Zumberge, J. Berger, J. Otero, and E. Wielandt, Bull. Seismol. Soc. Am. **100**, 598 (2010).
26) J. Berger, P. Davis, R. Widmer-Schnidrig, and M. Zumberge, Bull. Seismol. Soc. Am. **104**, 2422 (2014).
27) A. Araya, Tech. Res. Rep. (ERI, Univ. Tokyo) **1**, 1 (1996) [in Japanese].
28) K. Hotate, M. Enyama, S. Yamashita, and Y. Nasu, Meas. Sci. Technol. **15**, 148 (2004).
29) Y. Shindo, T. Yoshikawa, and H. Mikada, Proc. IEEE Sensors, 2002, Vol. 2, p. 1767.
30) Optical Fiber Accelerometer [http://www.mems-core.com/service/jirei/images/jirei03/AEsensor_catalog.pdf] [in Japanese].
31) *Jishin no Jiten*, ed. T. Utsu, E. Shima, T. Yoshii, and K. Yamashina (Asakura, Tokyo, 2001) 2nd ed., Chap. 2 [in Japanese].
32) H. Fujiwara, T. Kunugi, S. Adachi, S. Aoi, and N. Morikawa, Nihon Jishin Kogakkai Ronbunshu **7**, 2 (2007) [in Japanese].
33) T. Tomioka and S. Yamamoto, JET Tech. Rep. **29**, 1 (2006) [in Japanese].
34) P. L. M. Heydemann, Appl. Opt. **20**, 3382 (1981).
35) A. Barzilai, T. VanZandt, and T. Kenny, Proc. ASME Int. Congr., 1998, p. 15.
36) R. Brincker, T. L. Lago, P. Andersen, and C. Ventura, Proc. 23rd Int. Modal Analysis Conf. (IMAC), 2005.